Mechanism of C−O Activation in Dimethoxyethane Cationic Iron Complexes

Sophie Le Caër, Michel Heninger, Pascal Pernot, and Hélène Mestdagh*

Laboratoire de Chimie Physique (UMR 8000, CNRS/Université Paris-Sud 11), Bât. 350, Université Paris-Sud, 91405 Orsay Cedex, France

Received: July 29, 2005; In Final Form: April 14, 2006

The fragmentation mechanism of iron complexes bearing a bidentate ligand, dimethoxyethane (CH_3OCH_2-CH_2OCH_3, labeled as DXE) has been investigated by means of FT-ICR mass spectrometry (ion−molecule reactions) and infrared multiphoton dissociation spectroscopy. Two possible reaction mechanisms were envisioned for the $Fe(DXE)^+ + DXE$ reaction, leading to the formation of the $Fe(CH_2O)(DXE)^+$ ion. The two mechanisms differ in the nature of the neutral molecules formed: $CH_3OC_2H_5$ or $CH_2{=}CH_2 + CH_3OH$. The combination of ion−molecule reactions, thermochemistry considerations, and IRMPD spectra leads us to suggest that the mechanism involves successive elimination of the neutrals $CH_2{=}CH_2$ and CH_3OH, the first step of the mechanism being the insertion of the iron atom in the $O-C_{central}$ bond.

Introduction

Bidentate ligands are widely used in organometallic chemistry. Beyond the larger binding energy brought by the presence of a second binding site, the enhanced stability of the bidentate complexes is generally explained by the "chelate effect" related to the entropically favorable character of the complexation by a bidentate ligand compared to a monodentate one.[1] Geometrical constraints within a bidentate complex may also play a role in its specific reactivity. Under very dilute conditions such as those of low-pressure gas-phase ion−molecule reactions, the chelate effect may be viewed as the ability of partial decomplexation without complete loss of the ligand. In energetic terms, this means that a bidentate complex may accumulate a relatively large amount of internal energy without spending it immediately in metal−ligand dissociation. With internal energy increase, conformational changes may occur in relation with partial decomplexation. These features are expected to induce a specific reactivity in the bidentate complex. Moreover, this reactivity could be significantly dependent on its internal energy.

The successive reactions of iron carbonyl cations $Fe(CO)_n^+$ ($n = 1-4$) with oxygen-containing monodentate ligands such as water,[2,3] methanol[4] or dimethyl ether CH_3OCH_3 (DME)[5,6] have been studied in our group. The internal energy dependence in the $Fe(CO)^+ + O_2$ system, characterized by the corresponding radiative lifetime, was also reported.[7] The present article deals with the chemistry of iron complexes of 1,2-dimethoxyethane, $CH_3OCH_2CH_2OCH_3$ (DXE), the simplest bidentate analogue of dimethyl ether. While several studies have focused on the binding energy of DXE and polyethers with various cationic species such as H^+, NH_4^+,[8] and alkali cations,[9−11] and transition metal cations such as Co^+, Ni^+, and Cu^+,[12,13] little information is available on the specific reactivity of DXE complexes. The binding energies of metal cations have generally been determined using energy-controlled CID,[9] ligand exchange reactions,[13] or association reactions.[10,11] These studies show that the binding energies in the polydentate complexes increase with increasing ligand size and the number of available oxygen groups, and that due to the geometrical constraints the binding energy of DXE is less than twice that of DME.

The reaction of FeL^+ with the ligand L, where L = methanol or DME, involves C−O cleavage. In the case of the DME ligand,[5] we have proven that a competition between homolytic cleavage ($CH_3^\bullet$ loss) and cleavage with rearrangement (CH_4 loss) takes place. The branching ratio between these two channels is strongly energy-dependent, the latter channel being preferred (up to 60%) at low internal energies. We have recently reported the experimental IRMPD (infrared multiphoton dissociation) spectra and calculated structures of $Fe(DME)_2^+$, $Fe(DXE)^+$, and $Fe(DXE)_2^+$.[14] These results show that in the most stable form of the complexes no metal insertion in the C−O bond occurs, and that in both DXE complexes the DXE ligands are bound by two oxygen atoms. The fragmentation products of $Fe(DME)_2^+$ correspond to 85% CH_4 loss along with 15% $CH_3^\bullet$ loss. Since IRMPD is known to lead in most cases to the lowest energy dissociation channel,[15] this is fully consistent with the reactivity trends in the $Fe(DME)^+$/DME system. The IRMPD fragmentation mode of DXE complexes $Fe(DXE)^+$ and $Fe(DXE)_2^+$ is completely different from $Fe(DME)_2^+$ fragmentation, since it loses ethene.

The aim of the present work is (i) to investigate the fragmentation mechanism in DXE complexes and (ii) to probe the excited $Fe(DXE)_2^+$ system, termed as $Fe(DXE)_2^{+}$*, at a higher energy content than with IRMPD. To this end we have studied the reactivity of DXE with more or less energetic $Fe(DXE)^+$ reactant ions, using kinetic analysis of the successive reactions in the $Fe(CO)_2^+ + DXE$ system. To explore intermediate energy contents, we have also studied the reactivity of the $Fe(CO)(DXE)^+ + DXE$ system. This system is probed at low energy using the IRMPD study of the $Fe(CO)(DXE)_2^+$ ion. This new IRMPD spectrum is included here.

Experimental Methods and Data Analysis

1. Ion—Molecule Reactions: The Experimental Setup. The triple cell FT-ICR spectrometer "Tricyclotron" used in this study has been described previously.[16] It consists of three ion traps which are differentially pumped. The first trap is used as an ion source. The second, maintained at a low residual pressure, is alternatively used for relaxation of ions before reaction and as a detection cell. The third is the reaction zone. Efficient

* Corresponding author. E-mail: helene.mestdagh@lcp.u-psud.fr.

10.1021/jp054202z CCC: $33.50
Published on Web 07/18/2006

differential pumping ensures a pressure drop by a factor 250 between the central cell and the two adjacent cells. This configuration allows to perform ion−molecule reactions at thermal kinetic energy.[17,18]

The three cascaded ICR cells are immersed in the same magnet: ions can thus be transferred from one ion trap to the next with a drift velocity perpendicular to the magnetic field. The drift velocity is small compared with the thermal velocity, so that the ions do not gain kinetic energy when drifted from one cell to the next. The ions can be stored successively in each trap for a well controlled time. The time needed to transfer the ions from one cell to the next is in the millisecond range.

The $Fe(CO)_2^+$ ions are produced in the first cell (source) by electron ionization of $Fe(CO)_5$ at a typical pressure of 10^{-5} Torr using a 20 eV electron beam. The $Fe(CO)_2^+$ ions are then isolated by selective ejection of all the other ions. The mass-selected ions are then drifted to the second cell, where they may be stored for a variable time, and transferred to the third cell where they react with dimethoxyethane at a typical pressure of $(1-2) \times 10^{-6}$ Torr. The reaction time was varied between 1 and 800 ms. After reaction, the ions are drifted back to the second cell for FT-ICR detection. The collisional relaxation experiments were performed by adding argon at a typical pressure of $(3-30) \times 10^{-5}$ Torr in the reaction cell.

Radiative relaxation in the second cell allows thermalization of the internal and/or kinetic energy of the reactant ions, as electron ionization is known to produce excited ions. Using a monitor reaction, radiative lifetimes or cooling rate constants of excited ions can be derived.[19,17,18] The effect of $Fe(CO)_2^+$ radiative relaxation was studied by trapping the $Fe(CO)_2^+$ reactant ions for a variable time (0−1200 ms) in the second cell before reaction, keeping the pressure and the reaction time in the third cell constant during the experiment. In the second cell, the typical pressure is ca. 2×10^{-8} Torr and the residual gas is mainly water, which corresponds to ca. 1 collision per second. Therefore, the relaxation of ions observed in the second cell can be considered as mainly radiative. Collisional relaxation is competitive only for cooling times longer than ca. 1 s.

2. Ion—Molecule Reactions: Data Analysis and Kinetic Modeling. The intensity of each ion signal, normalized to the total ion signal (sum of the ions with significant intensity) is plotted as a function of the reaction time.

The rate constants of the different processes are obtained using the KINET program as described previously.[5] As explained in the discussion part, a given reaction may be represented by several steps with different rate constants. This allows energy-dependent reactions to be taken into account. The program allows a global optimization of the parameters. All abundance curves of an experiment are treated simultaneously with a global analysis method based on the transfer matrix for a set of pseudo-unimolecular reactions.[20] Apparent rate constant mean values and standard deviations are determined by Bayesian data analysis of the complete set of time-resolved species abundances.[21] To account for the transfer times of ions to and from the reaction cell, a small negative time shift is introduced in the data analysis and optimized like the other parameters. For all of the experiments the resulting time shift values were within the expected range, 0.3−0.8 ms.

For several of the ion−molecule reactions the rate constants are compared with the capture rate constants, which were evaluated according to Su and Chesnavich.[22] This method requires the knowledge of the polarizability and the dipole moment of the DXE molecule. The former is evaluated at 9.5 $Å^3$ either from the polarizabilities of linear alkane and ether molecules, or by adding the atomic polarizabilities.[23] The dipole moment of DXE in the gas phase has been calculated as an average of the dipole moments of the different conformers of DXE, weighted according to their respective population at room temperature.[24] We used this theoretical value of 1.6 D, which is in agreement with the experimental dipole moment of DXE in low polarity solvents.

3. IRMPD Spectroscopy. The IRMPD spectroscopy of ions[25] was performed using the coupling of the Free Electron Laser (FEL) CLIO at Orsay[26] with MICRA, a compact and easily transportable FT-ICR mass spectrometer developed in our laboratory.[27] This instrument, based on a structured permanent magnet with 1.24 T nominal field, is very well suited for temporary coupling to a FEL. The tuning range 110−3300 cm^{-1} is available with the FEL CLIO. Nevertheless, only the region from 800 to 2200 cm^{-1} is used in the present experiments. The FEL temporal structure consists of macropulses of 8 μs duration, at a repetition rate of 25 Hz. Each macropulse contains a series of 1−2 ps micropulses at a repetition rate of 62.5 MHz. A macropulse contains up to 40 mJ of energy, with a peak power of 40 MW in each micropulse. The infrared light is focused in the center of the ICR cell with a 1 m focal length mirror. The beam alignment and mirror position have been set so as to optimize the photofragmentation rates of $Fe(CO)_5^+$.

The ions of interest are prepared in the FT-ICR cell by a sequence including pulsed $Fe(CO)_5$ admission, electron ionization of $Fe(CO)_5$, mass selection of the $Fe(CO)_n^+$ ions, DXE admission, ion−molecule reaction and mass selection of the desired ions. A relaxation delay of 500−1000 ms is allotted before irradiation. The ions are then irradiated for a definite time, and the resulting ions are detected. The sequence ends with a quench, i.e., ejection of all the ions from the cell. Such a sequence is repeated 20 times, and the mass spectrum is the Fourier transform of the accumulated ion signal. The IR laser wavelength is increased by 10 cm^{-1} between two consecutive points and the same procedure is repeated at each successive wavelength. For each mass spectrum the intensities of the parent and fragment ions are corrected if necessary from the average noise taken from a blank spectrum and normalized to the sum of the intensities of significant ions. The global infrared spectrum is obtained by plotting the fragmentation efficiency defined as $-\ln(I_{parent})$, where I_{parent} is the relative intensity of the parent ion, as a function of the wavelength. The corresponding product-resolved spectrum is the wavelength dependence of the relative abundances of each fragment.

4. Theoretical Methods. Theoretical calculations were performed with the GAUSSIAN 98 suite of programs[28] using the B3LYP hybrid density functional. For iron, we used the [8s6p4d1f] contraction of the (14s11p6d3f) primitive basis set as recommended by Bauschlicher.[29] A polarized double-ζ basis set was used for the ligands.[30] All the structures calculated were characterized as minima.

5. Synthesis of Deuterated DXE, $CD_3OCH_2CH_2OCD_3$. To check the origin of H atoms, the deuterated dimethoxyethane $CD_3OCH_2CH_2OCD_3$ (labeled as dDXE) was synthesized as follows from ethylene glycol and trideuterated iodomethane, using a modification of the general procedure.[31,32] First, 40 mmol of powdered KOH was added to 20 mL of dimethyl sulfoxide. The mixture was stirred at room temperature for 5 min. Then 5 mmol of ethylene glycol immediately followed by 12 mmol of CD_3I were added. The mixture was stirred for 30 min and filtered. The filtrate was then distilled. The product was then characterized by mass spectrometry and ^1H NMR (200 MHz). Its isotopic purity was better than 98% d_6.

Results and Discussion

1. Ion—Molecule Reactions. Kinetic studies of ion−molecule reactions were performed using a triple cell Fourier transform ion cyclotron resonance (FT-ICR) mass spectrometer, particularly suited for following the kinetics of successive ion−molecule reactions and for varying ion relaxation.[16] The data were plotted as abundance curves giving the relative intensity of each ion, characterized by its *m*/*z* ratio, as a function of reaction time. To derive the rate constants of the successive processes, the data were analyzed using the KINET program allowing global treatment of each set of abundance curves in a bayesian data analysis framework.[5] This method provides the set of rate constants for a given kinetic scheme, along with information about possible parametric identifiability problems. This term refers to the situation where the optimum set of parameters (rate constants in the present case) is not unique. This point is crucial within the model we have developed for kinetic analysis of energy-dependent reactions, which is based on the use of kinetic schemes where a given observed transformation is represented by more than one kinetic step. If such a scheme is overparametrized, it may lead to a whole family of optimal solutions where some of the rate constants strongly depend from each other and correspond in fact to a large range of possible values. The bayesian method addresses this specific problem and supplies a confidence interval for each of the parameters included in the kinetic scheme, along with the correlation patterns existing between the parameters, including nonlinear correlations.

Despite its limitations, our approach to the modeling of energy-dependent reactions is considerably lighter in terms of calculations than explicitly introducing continuous energy distributions of ions and energy dependences of the rate constants. For complex reaction schemes, it appears as a convenient alternative to the explicit modeling of energy distribution with master equation formalism.[33,34] The latter approach is more accurate but requires one to locate all the transition states involved in the process and to evaluate their vibrational frequencies, which is not trivial for transition metal systems.

1.1. Reactivity of $Fe(CO)^+$ with DXE: Qualitative Results. The reaction of $Fe(CO)^+$ with DXE yields four primary products, and leads rapidly to complex reaction mixtures on further reaction with DXE. These primary products correspond to *m*/*z* 118, 103, 100, and 146, by decreasing the order of relative initial rate of formation. The latter one is $Fe(DXE)^+$ resulting from substitution of CO by a DXE molecule, and the three major products result from fragmentation of excited $Fe(DXE)^+$: $[Fe, C_2, H_6, O_2]^+$ (*m*/*z* 118), $[Fe, C, H_3, O_2]^+$ (*m*/*z* = 103), and $[Fe, C_2, H_4, O]^+$ (*m*/*z* 100) correspond respectively to ethene loss, $[C_3, H_7]$ loss, and $[C_2, H_6, O]$ loss from $Fe(DXE)^+$. Dissociation of metastable $Fe(DXE)^+$ in a magnetic sector mass spectrometer also involves ethene loss as a major pathway.[35] Similarly, IRMPD fragmentation of $Fe(DXE)^+$ involves ethene loss.[14] The *m*/*z* 118 ion resulting from $[Fe(DXE)^+]^*$ is probably the same as the intermediate involved in decomposition of metastable dimethylperoxide complex $Fe^+(CH_3OOCH_3)$, which yields *m*/*z* 103 and 100 fragment ions.[36] Our assignment on the molecular formulas of the *m*/*z* 103 and 100 ions has been done in analogy with this (dimethylperoxide + Fe^+) chemistry. The branching ratio between the primary products from $Fe(CO)^+$/DXE varies with reaction time, in particular the relative importance of $Fe(DXE)^+$ formation increases with increasing time. This is consistent with collisional cooling of excited $Fe(DXE)^+$ competing with its fragmentation, so that $Fe(DXE)^+$ can be stabilized after a sufficient number of collisions.

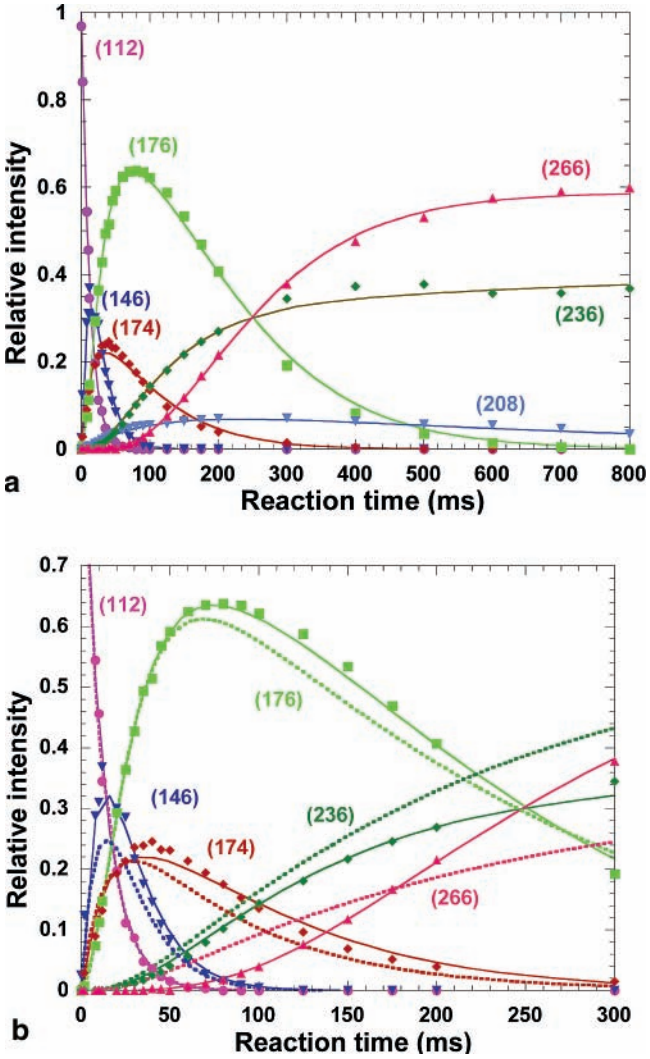

Figure 1. (a) Dependence of ion distribution with reaction time for the reaction of $Fe(CO)_2^+$ with DXE (reaction pressure: 1.3×10^{-6} Torr): abundance curves of all the ions. Solid lines are fits according to Scheme 2 as explained in text. The *m*/*z* ratio is given into brackets. (b) Dependence of ion distribution with reaction time for the reaction of $Fe(CO)_2^+$ with DXE (reaction pressure: 1.2×10^{-6} Torr): Fit of the DXE reaction using a simple kinetic scheme (dashed lines) compared with the advanced fit (solid lines). For clarity, the *m*/*z* 208 ion is not shown, nor the time and intensity range above 300 ms and 0.7, respectively.

Because of the complexity of the reaction scheme, joined to the strongly energy-dependent reactivity, no quantitative kinetic study was undertaken on the $Fe(CO)^+$ + DXE system. Clearly this system is not suited to our purpose, since the substitution of CO by DXE is so exothermic that most of the $Fe(DXE)^+$ ions produced are above their fragmentation threshold.

Therefore, we have focused on the reactivity of $Fe(CO)_2^+$ with dimethoxyethane.

1.2. Reactivity of $Fe(CO)_2^+$ with DXE: Nature of the Products. The time dependence of the relative abundances of reactant and product ions is shown in Figure 1a. The ion distribution observed at short reaction time shows two primary products, resulting from substitution of one or two CO molecules by DXE: $Fe(CO)DXE)^+$ (*m*/*z* 174) and $Fe(DXE)^+$ (*m*/*z* 146). These ions lead to $[Fe, C_5, H_{12}, O_3]^+$ (*m*/*z* 176), $[Fe, C_6, H_{16}, O_4]^+$ (*m*/*z* 208), and $[Fe, C_8, H_{20}, O_4]^+$ (*m*/*z* 236, $Fe(DXE)_2^+$) ions. At longer reaction times ion $[Fe, C_9, H_{22}, O_5]^+$ (*m*/*z* 266)

TABLE 1: Proposed Connectivities for the Different Ions Observed in the $Fe(CO)_2^+$ + DXE System, Based on the Mass Differences between Corresponding Ions in the dDXE and DXE Systems, Where the Hydrogen Atoms Replaced by D in the dDXE System Are Indicated by Bold Characters

m/z in DXE system	*m/z* (dDXE) − *m/z* (DXE) difference	proposed structure
146	6	$Fe(C\mathbf{H_3}OCH_2CH_2OC\mathbf{H_3})^+$
174	6	$Fe(CO)(C\mathbf{H_3}OCH_2CH_2OC\mathbf{H_3})^+$
176	8	$Fe(C\mathbf{H_2}O)(C\mathbf{H_3}OCH_2CH_2OC\mathbf{H_3})^+$
208	12	$Fe(OC\mathbf{H_3})_2(C\mathbf{H_3}OCH_2CH_2OC\mathbf{H_3})^+$
236	12	$Fe(C\mathbf{H_3}OCH_2CH_2OC\mathbf{H_3})_2^+$
264	12	$Fe(CO)(C\mathbf{H_3}OCH_2CH_2OC\mathbf{H_3})_2^+$
266	14	$Fe(C\mathbf{H_2}O)(C\mathbf{H_3}OCH_2CH_2OC\mathbf{H_3})_2^+$

is formed from *m/z* 176 by DXE association. Ion $Fe(CO)(DXE)_2^+$ (*m/z* 264) resulting of DXE association to $Fe(CO)(DXE)^+$, is also detected in very minor amount (not shown in Figure 1a).

To check the origin of H atoms, the ions produced in the $Fe(CO)_2^+$ + DXE and in the $Fe(CO)_2^+$ + dDXE system were compared. The abundance curves obtained in the case of $Fe(CO)_2^+$ reacting with dDXE are very similar to those of DXE depicted in Figure 1a, except that the corresponding *m/z* values are shifted. Each product from dDXE appears as a single *m/z* value, indicating that in the course of the successive reactions no scrambling occurs between the central H and terminal D atoms.

Table 1 shows the mass differences between the $Fe(CO)_2^+$ + DXE and the $Fe(CO)_2^+$ + dDXE systems. For example, the *m/z* 176 ion with DXE becomes *m/z* 184 with dDXE. The $Fe(CH_2O)(DXE)^+$ structure was then attributed to this ion, the methanal ligand coming from a terminal carbon atom in the dimethoxyethane. The *m/z* 208 ion becomes *m/z* 220 with dDXE, indicating that it includes four terminal methyl groups from DXE. This suggests an $Fe(OCH_3)_2(DXE)^+$ or related structure. This ion is probably an analogue of the *m/z* 118 ion obtained in the $Fe(CO)^+$ + DXE system, with an additional DXE ligand. An accurate study of *m/z* 118 ion from $Fe(CH_3OOCH_3)^+$ has shown that the initially formed structure $Fe(OCH_3)_2^+$ is easily isomerized into $Fe(OCH_2)(CH_3OH)^+$.[36] Moreover, the corresponding activation barrier may be significantly lowered by the presence of an additional ligand, as demonstrated in a similar case of isomerization, namely $Fe(OCH_3)^+$ to $HFe(OCH_2)^+$.[37] Thus, the *m/z* 208 ion may have either or both of the two isomeric structures $Fe(OCH_3)_2(DXE)^+$ and $Fe(OCH_2)(CH_3OH)(DXE)^+$. In the following, it will be written as $Fe(OCH_3)_2(DXE)^+$.

The product formulas and the shape of the abundance curves suggest the reaction scheme depicted in Scheme 1. Channel 1a corresponds to primary formation of $Fe(DXE)^+$ which gives exclusively $Fe(CH_2O)(DXE)^+$ through reaction with DXE, while channel 1b corresponds to $Fe(CO)(DXE)^+$ which leads to various products. This filiation scheme was confirmed by continuous selective ejection experiments.[5]

At this stage alternative schemes are also conceivable, particularly concerning the *m/z* 208 ion for which the selective ejection experiments were inconclusive due to its low amount. As will be shown in the following, this particular reaction scheme has been chosen because of its consistency with the whole set of experimental data.

Fitting of the kinetics of these successive reactions was initially tried out by using the simple kinetic scheme obtained by assignment of a rate constant to each of the successive and parallel steps of the reaction scheme. The result is depicted in Figure 1b (zoom of some significant ions of Figure 1a), showing that this simple fit is not appropriate. Use of a simple kinetic law with other conceivable reaction schemes could not fit the experimental data either. This indicates that the reactivity of the ions involved is strongly energy-dependent, as already observed in the chemistry of dimethyl ether cationic iron complexes. Therefore, the rate constants appear as time-dependent, since the reactions of a given ion compete with collisional relaxation which decreases its energy. For instance, the *m/z* 266 ion $Fe(CO)(DXE)_2^+$, resulting from DXE association to $Fe(CO)(DXE)^+$, appears with a time lag so that its short time dependence is not accounted for by the simple kinetic fit. This is due to the fact that the $Fe(CO)(DXE)^+$ ions cannot undergo efficient association as soon as they are formed, because they are hot since they arise from an exothermic substitution reaction. The method used to take this energy dependence into account in the kinetic modeling has been previously described.[5] It is based on the representation of an intermediate ion by two or more species with different reactivities, corresponding to different average internal energies. In the kinetic scheme, these species are successively converted to each other through relaxation steps. Obtaining an adequate fit of the experimental curves requires that three species are used for $Fe(CO)(DXE)^+$, as for $Fe(CH_2O)(DXE)^+$. The reactivity of the former ion is remarkably dependent on the energy, since it leads to four different products: $Fe(CH_2O)(DXE)^+$, $Fe(OCH_3)_2(DXE)^+$, $Fe(DXE)_2^+$, and $Fe(CO)(DXE)_2^+$, seemingly in decreasing order of $Fe(CO)(DXE)^+$ average energy.

SCHEME 1: Ion−Molecule Reactions Observed in the $Fe(CO)_2^+$ + DXE System

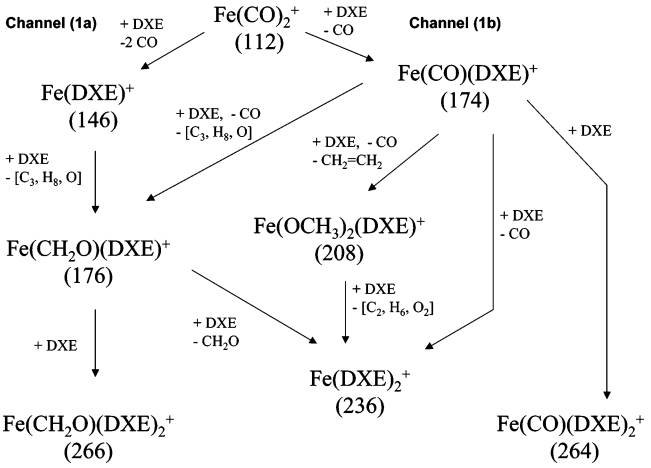

To confirm this hypothesis and to get more information about the energy dependence of the reactivity, the reaction was performed under different conditions of collisional and radiative relaxation.

1.3. Radiative Relaxation of $Fe(CO)_2^+$. Studying the dependence of product distribution with the relaxation time of the $Fe(CO)_2^+$ reactant ions gives us qualitative information on the energy dependence of the primary reaction and an estimation of the characteristic time associated with radiative cooling of the $Fe(CO)_2^+$ ions resulting from electron ionization.

These experiments are performed by varying the relaxation time allowed to the $Fe(CO)_2^+$ reactant ions trapped in the second cell of the FT-ICR instrument before they are transferred to the third cell for reaction. The relaxation of the $Fe(CO)_2^+$ ions trapped in the second cell proceeds mainly by radiative cooling, since this cell is maintained at very low pressure. The third cell contains DXE at a constant pressure of 1.0×10^{-6} Torr. The reaction time of the $Fe(CO)_2^+$ ions with DXE in this cell is

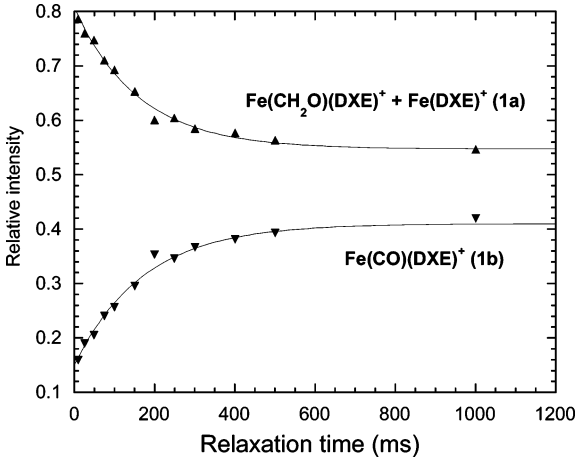

Figure 2. Dependence of $Fe(CO)(DXE)^+$ (▼) and $Fe(DXE)^+$ with its daughter ion $Fe(CH_2O)(DXE)^+$ (▲) with the relaxation time of $Fe(CO)_2^+$ ions in the second cell.

kept constant, equal to 50 ms, while the relaxation time in the second cell is varied up to 1 s. Note that contrary to the experiments described in the preceding section, these experiments do not involve following the reaction progress, but use a fixed reaction time corresponding to incomplete consumption of the reactant. Therefore, unreacted parent ions remain present for all values of the relaxation time. Under these conditions, the only ions observed are $Fe(CO)_2^+$, $Fe(DXE)^+$, $Fe(CO)(DXE)^+$ and $Fe(CH_2O)(DXE)^+$. The relative intensity of $Fe(CO)_2^+$ ions is constant and equal to 0.05, whatever the relaxation time. Ion $Fe(DXE)^+$ is formed faster than $Fe(CO)(DXE)^+$ and is rapidly converted to $Fe(CH_2O)(DXE)^+$, so that we can estimate that the $Fe(CH_2O)(DXE)^+$ ion present at this stage arises from $Fe(DXE)^+$ through channel (1a), while $Fe(CO)(DXE)^+$ has not yet reacted significantly. The sum of the relative intensities $I_{Fe(DXE)^+} + I_{Fe(CH_2O)(DXE)^+}$, is therefore proportional to the relative importance of channel 1a, while the relative intensity $I_{Fe(CO)DXE^+}$ is proportional to channel 1b. Figure 2 depicts the evolution of these two channels with $Fe(CO)_2^+$ relaxation time.

Channel (1a) decreases when the relaxation time increases, suggesting that these ions are issuing from excited $Fe(CO)_2^+$*. The sum of the relative intensities $I_{Fe(DXE)^+} + I_{Fe(CH_2O)(DXE)^+}$ is directly related to the proportion of ions having enough internal energy to lead to $Fe(DXE)^+$, after a double substitution. Assuming that the average energy of parent ions decreases exponentially as a function of the relaxation time, the $I_{Fe(DXE)^+} + I_{Fe(CH_2O)(DXE)^+}$ sum decreases according to an exponential. As the sum of the intensities of the ions is equal to 1, the dependences of the relative intensities of the different ions against the relaxation time t can be fitted by the following expressions:

$$I_{Fe(CO)_2^+} = A = 0.05$$

$$I_{Fe(DXE)^+} + I_{Fe(CH_2O)(DXE)^+} = B + C\exp\left(-\frac{t}{\tau}\right)$$

$$I_{Fe(CO)(DXE)^+} = (1 - A - B) - C\exp\left(-\frac{t}{\tau}\right)$$

As shown in Figure 2, this model accounts for the experimental curves. The fit leads to a characteristic radiative cooling time $\tau = 170 \pm 50$ ms.

It may seem surprising that the relative intensity of $Fe(CO)_2^+$ ions does not depend on the relaxation time, which means that the global rate constant for the sum of the two channels is not energy-dependent. As a possible explanation, both channels probably begin with the same step: substitution of one CO leading to $Fe(CO)(DXE)^+$* which may fragment or not depending on its internal energy, itself related to the internal energy of $Fe(CO)_2^+$ reactant:

$$Fe(CO)_2^+* + DXE \rightarrow Fe(CO)(DXE)^+* + CO$$

This reaction is strongly exothermic (as CO is replaced by a bidentate ligand). Its rate constant likely remains close to the capture rate constant and does not depend on the energy of reacting $Fe(CO)_2^+$. Consistently with this hypothesis, we find that the global rate constant for $Fe(CO)_2^+$ decay is 15.0×10^{-10} $cm^3 \cdot molecule^{-1} \cdot s^{-1}$, i.e., 99% of the capture rate constant $k_C(Fe(CO)_2^+ + DXE) = 15.2 \times 10^{-10}$ $cm^3 \cdot molecule^{-1} \cdot s^{-1}$.

SCHEME 2: Kinetic Scheme of the $Fe(CO)_2^+ + DXE$ System Used Whatever the Argon Pressure[a]

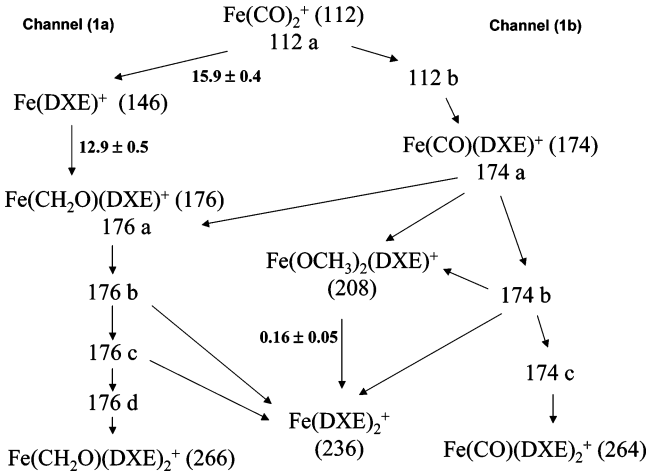

[a] The *m/z* ratio of the different ions is indicated in brackets. The rate constants for zero argon pressure are expressed in 10^{-10} $cm^3 \cdot molecule^{-1} \cdot s^{-1}$, along with their uncertainties. Two or more species (for the same ion) labeled as a, b, ..., of different reactivities are used, when necessary, in order to get a good agreement between experimental and fitted curves.

1.4. Cooling the Reaction Mixture with Argon. To adjust the average energy contents of the reactant and intermediate ions, the reaction mixture was cooled with argon by using a variable argon pressure. Increase of the argon pressure has a dramatic effect on the shape of the abundance curves, leading for example to a strong decrease of the $Fe(CH_2O)(DXE)^+$ intensity.

All the sets of curves corresponding to different argon pressures can be modeled using the same kinetic scheme, outlined in Scheme 2. In this scheme, some of the ions are represented by several species designated as a, b, ..., representing decreasing energy content. These species concurrently undergo collisional cooling, for instance from a to b, and reaction leading to other chemical species. The number of intermediates used for a given mass results from a compromise between two requirements: obtaining a satisfactory fit and avoiding non-identifiability of the parameters. Note that the bayesian method supplies accurate information on both of these points. For instance, it reveals a strong correlation between the individual rate constants of successive collisional cooling steps, which could be expected since the intermediate species are only defined by their decreasing average energy. Thus, the values of these rate constants have little meaning and are not mentioned in Scheme 2. To get essential information about an energy-

dependent reaction, it is preferable to derive average rate constants for each reaction channel, as described further for the $Fe(CO)DXE^+$ ion.

The set of rate constants was separately optimized for each argon pressure. For some of the reactions the rate constants found for the different argon pressures are very similar, lying within a ±30% range in comparison with zero argon pressure. This indicates that these reactions are not very energy-dependent. Only the corresponding rate constants appear on Scheme 2. In contrast, the rate constants of the steps involved in energy-dependent reactions were found to depend strongly on the argon pressure. Among these, the rate constants of the collisional relaxation steps increase with argon pressure, i.e., with collision frequency. The (1a)/(1b) branching ratio decreases when the argon pressure increases, as expected since the direct substitution of two CO by one DXE requires more energy than the substitution of one CO.

The reactivity of $Fe(CO)(DXE)^+$ ions was particularly examined. Since the individual rate constants for energy-dependent species have no direct chemical meaning, we evaluated the average rate constant for each channel as described in the following. The channel leading to ion 208, $Fe(OCH_3)_2(DXE)^+$, will be taken as an example. This channel is the most complicated one in the kinetic scheme relative to $Fe(CO)(DXE)^+$, since 208 ions are formed both from 174a and 174b species of $Fe(CO)(DXE)^+$ ions. The average rate constant $\langle k_{208} \rangle$ is the sum of two terms: one is the individual rate constant for the 174a → 208 step, the other corresponds to the rate of the global transformation 174a → 174b → 208 and can be calculated from the individual rate constants at the argon pressure considered. The other average rate constants $\langle k_{176} \rangle$, $\langle k_{236} \rangle$ and $\langle k_{264} \rangle$ involving the transformations 174a → 176, 174a → 174b → 236, and 174a → 174b → 174c → 264, respectively, are determined similarly.

For each product ion and each argon pressure we also evaluated the average number of collisions N_c undergone by $Fe(CO)(DXE)^+$ before leading to this particular product.[2,3] For a given argon pressure N_c depends on the nature of the product ion: it increases in the order 176, 208, 236, 264; i.e., N_c is smaller for the products formed from hotter ions. The average rate constants are plotted against the corresponding average number of collisions and are represented in Figure 3.

The average rate constant of the channel leading to 176 decreases with increasing number of collisions, and this channel disappears completely at high N_c. This suggests that formation of $Fe(CH_2O)(DXE)^+$ from $Fe(CO)(DXE)^+$ is an endothermic reaction. By contrast, the average rate constant of simple CO substitution leading to $Fe(DXE)_2^+$ (*m*/*z* 236) increases with increasing N_c, while the rate constant of formation of *m*/*z* 208 ion is nearly independent of N_c. The relative importance of the association reaction leading to $Fe(CO)(DXE)_2^+$ (*m*/*z* 264) increases steadily with increasing N_c, as could be expected for an association reaction involving collisional stabilization of the excited intermediate.

These results suggest that the energy contents required for the four reaction channels of $Fe(CO)(DXE)_2^+$ increase in the following order:

$$Fe(CO)(DXE)_2^+ < Fe(DXE)_2^+ < Fe(OCH_3)_2(DXE)^+ < Fe(CH_2O)(DXE)^+$$

The sum of the average rate constants relative to the three nonassociative reaction channels undergoes little variation on the whole pressure range, in contrast with the branching ratio between these channels. A possible interpretation lies in rate-determining initial CO substitution by DXE leading to $Fe(DXE)_2^+$*, whose evolution depends on its internal energy. The corresponding CO substitution rate constant (sum of the nonassociative rate constants: $(4-4.6) \times 10^{-10}$ $cm^3 \cdot s^{-1}$) is only about one-third of the capture rate constant $k_C(FeCODXE^+ + DXE) = 1.38 \times 10^{-9}$ $cm^3 \cdot s^{-1}$. This indicates that ca. two-thirds of the collisions are either unreactive or correspond to substitution of the DXE ligand by another DXE molecule.

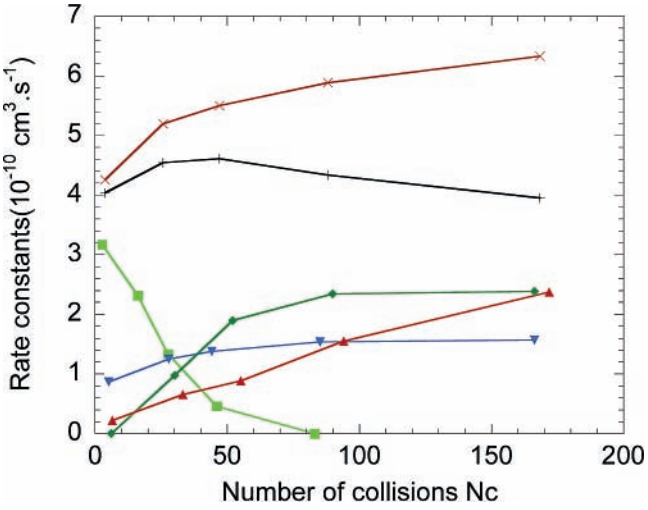

Figure 3. Dependence of the average rate constants with the average collision number N_c (see text) undergone by the $Fe(CO)(DXE)^+$ ions before they react with DXE: *m*/*z* 176, $Fe(CH_2O)(DXE)^+$ (green square); *m*/*z* 208, $Fe(OCH_3)_2(DXE)^+$ (red triangle); *m*/*z* 236, $Fe(DXE)_2^+$ (green tilted square); *m*/*z* 264, $Fe(CO)(DXE)_2^+$ (blue triangle); sum of all rate constants (×); sum of all rate constants without association reactions (+).

The preceding considerations are also consistent with the reactivity of $Fe(CH_2O)(DXE)^+$ and the corresponding kinetic scheme involving collisional relaxation: substitution of CH_2O by DXE in "hot" $Fe(CH_2O)(DXE)^+$ gives $Fe(DXE)_2^+$* with a high energy content, which leads back to $Fe(CH_2O)(DXE)^+$ with the neutral losses discussed further on. Therefore, collisional relaxation of $Fe(CH_2O)(DXE)^+$ increases its reaction rate to $Fe(DXE)_2^+$.

2. IRMPD Fragmentation of the Complexes of Interest. The IRMPD spectroscopy of selectively prepared gas-phase ions has been made possible by the coupling of a mobile FT-ICR mass spectrometer with the infrared free electron laser (FEL) CLIO.[25] Other IR spectra of gas-phase ions were reported using this instrument[14,38−41] or the FEL FELIX.[42−45] Irradiation of mass-selected ions at a given wavelength leads to multiphoton absorption resulting in ion fragmentation, if this wavelength is absorbed by the ion. The nature and relative amount of the fragments are monitored by mass spectrometry. The wavelength dependence of the fragmentation amount provides the IR spectrum of the ion.

2.1. $Fe(DXE)_2^+$. The $Fe(DXE)_2^+$ ions were irradiated for 500 ms with photons of wavelength ranging from 800 to 2000 cm^{-1}. The IR spectrum obtained (appearing as dashed line in Figure 6) has already been reported.[14] Under the conditions used (full laser power) three photofragment ions were observed: $Fe(CH_2O)(DXE)^+$, $Fe(OCH_3)_2(DXE)^+$, and $Fe(DXE)(H)^+$ in smaller amounts. Dividing the laser power by nine by using two attenuators leads to the fragment-resolved spectrum depicted in Figure 4, showing only the strongest absorption band.

Under these conditions $Fe(OCH_3)_2(DXE)^+$ remains the major fragment, while $Fe(DXE)(H)^+$ is not detected. This suggests

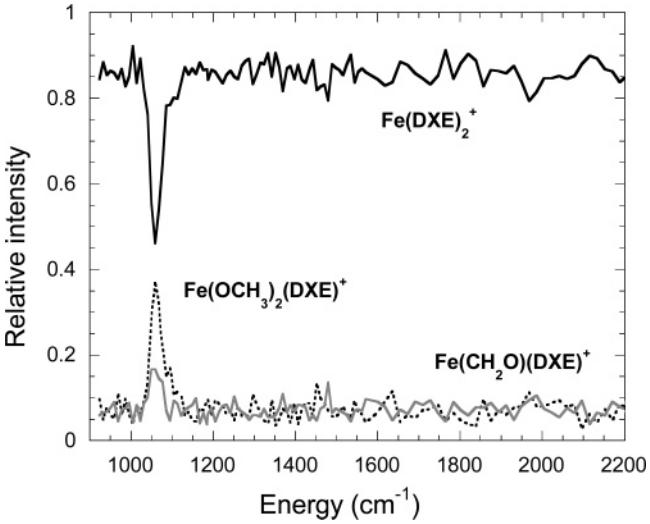

Figure 4. Relative intensity of the different ions as a function of the wavenumbers using a set of two attenuators, which divide the laser power by nine. The intensity of the parent ion $Fe(DXE)_2^+$ is represented in black; the intensities of the two photofragment ions observed, $Fe(OCH_3)_2(DXE)^+$ and $Fe(CH_2O)(DXE)^+$, are respectively represented as dashed and gray lines.

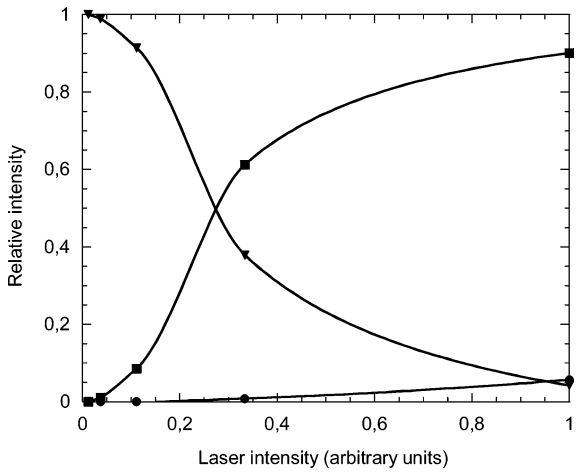

Figure 5. Relative intensity of the different photofragments resulting from $Fe(DXE)_2^+$ as a function of the laser intensity: *m/z* 147, $Fe(H)(DXE)^+$ (●); *m/z* 176, $Fe(CH_2O)(DXE)^+$ (■); *m/z* 208, $Fe(OCH_3)_2(DXE)^+$ (▼). The lines are just interpolations of the experimental points.

that $Fe(OCH_3)_2(DXE)^+$ is the primary fragmentation product. It was confirmed by a separate experiment performed at a fixed wavelength of 1018 cm^{-1}, where the irradiation intensity was changed by varying attenuation. The evolution of the photofragment relative amount as a function of the irradiation intensity, depicted in Figure 5, shows that $Fe(OCH_3)_2(DXE)^+$ tends to be the only fragment at low intensity. In addition, photofragmentation of mass-selected $Fe(CH_2O)(DXE)^+$ ion performed at 1018 cm^{-1} allowed to check that this ion is not fragmented to $Fe(H)(DXE)^+$.

Therefore, we can suggest the following sequential fragmentation scheme:

$$Fe(DXE)_2^+ \rightarrow Fe(OCH_3)_2(DXE)^+ + CH_2{=}CH_2$$

$$Fe(OCH_3)_2(DXE)^+ \rightarrow Fe(CH_2O)(DXE)^+ + CH_3OH$$

$$\rightarrow Fe(H)(DXE)^+ + [C_2, H_5, O_2]^\bullet$$

The secondary fragmentation step is probably due to light reabsorption by $Fe(OCH_3)_2(DXE)^+$ Since the absorption bands

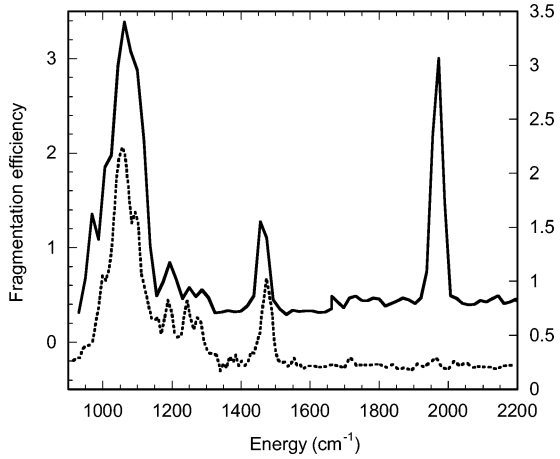

Figure 6. Infrared spectrum of $Fe(CO)(DXE)_2^+$. The infrared spectrum of $Fe(DXE)_2^+$ is given as a dashed line for comparison.

of $Fe(DXE)_2^+$ (a strong one between 1000 and 1100 cm^{-1}, and a weaker one around 1450 cm^{-1}) are characteristic of the DXE ligand, they should also exist at similar wavelengthes in the absorption spectrum of $Fe(OCH_3)_2(DXE)^+$, allowing this reabsorption. Unfortunately the IR spectrum of $Fe(OCH_3)_2(DXE)^+$ could not be recorded directly because of the very low relative abundance available for this ion.

Alternatively, it cannot be excluded that IRMPD of $Fe(DXE)_2^+$ produces some "hot" $Fe(OCH_3)_2(DXE)^+$ ions having enough internal energy to undergo further fragmentation. This might be due to the energy barrier required for reaching the transition state associated with ethene loss by the DXE ligand. Such an effect would likely be favored by a high laser power.

The branching ratio of the secondary fragmentation step clearly depends on the intensity of absorbed light, since $Fe(H)(DXE)^+$ is not formed at low intensity. A tentative mechanism involving the isomerization ability of the groups $Fe^+(OCH_3)_2$ [46] and $Fe^+{-}OCH_3$ [37] may be written as follows:

$$Fe(OCH_3)_2(DXE)^+ \leftrightarrows Fe(OCH_2)(CH_3OH)(DXE)^+$$

$$\rightarrow Fe(CH_2O)(DXE)^+ + CH_3OH$$

$$\rightarrow Fe(OCH_3)(DXE)^+ + [C, H_3, O]^\bullet$$

$$Fe(OCH_3)(DXE)^+ \leftrightarrows [HFe(OCH_2)(DXE)^+]^* \rightarrow$$

$$HFe(DXE)^+ + CH_2O$$

The [C, H_3, O]$^\bullet$ neutral formed from $Fe(OCH_3)_2(DXE)^+$ fragmentation may be either a methoxy radical $CH_3O^\bullet$ or a hydroxymethyl radical $^\bullet CH_2OH$. While the latter is more stable by 26 kJ mol^{-1},[47] the former seems to result from a more direct cleavage.

Homolytic methoxy (or hydroxymethyl) loss from $Fe(OCH_3)_2(DXE)^+$ probably requires significantly more energy than the pathway leading to $Fe(CH_2O)(DXE)^+$. This might explain why $HFe(DXE)^+$ is not observed under the "slow heating" conditions corresponding to low laser power.

2.2. $Fe(CO)(DXE)_2^+$. The $Fe(CO)(DXE)_2^+$ ions were prepared by reaction of mass-selected $Fe(CO)_n^+$ (n = 3 and 4) with DXE. Mass-selected $Fe(CO)(DXE)_2^+$ ions have been irradiated for 1240 ms with photons of wavelength ranging from 930 to 2200 cm^{-1}. The experimental spectrum for an average laser power of 550 mW is presented in Figure 6.

The characteristic features of both types of ligands appear on the spectrum: for wavenumbers below 1900 cm^{-1} a strong

TABLE 2: Band Positions and Relative Intensities of the Experimental IRMPD Spectra of $Fe(DXE)_2^+$ and $Fe(CO)(DXE)_2^+$ Ions, along with an Approximate Description of Each Mode

$Fe(DXE)_2^+$ [7]		$Fe(CO)(DXE)_2^+$			
				tentative assignment	
position (cm^{-1})	relative intensity	position (cm^{-1})	relative intensity	ligand	type of vibration
1056	1.00	1062	1.00	DXE	$C_{terminal}$−O stretching
1188	0.20	1193	0.20	DXE	CH_2 twist; CH_3 rock
1244	0.20	1249	0.10	DXE	CH_2 twist; CH_3 rock
1275	0.15	1287	0.10		
1473	0.40	1456	0.33	DXE	CH_3 deformation; CH_2 scissoring
		1972	0.88	CO	C═O stretching

similarity is observed between the spectra of $Fe(CO)(DXE)_2^+$ and $Fe(DXE)_2^+$, while the spectrum of the former presents an additional band at 1972 cm^{-1}, i.e., in the C═O stretching region.

Table 2 presents the positions and relative intensities of the different bands observed. Although no quantum chemical calculations were performed on $Fe(CO)(DXE)_2^+$, the assignment of the vibration modes can be made from comparison with the $Fe(DXE)_2^+$ spectrum, in which the bands were assigned using the theoretical spectrum from ab initio calculations.[14]

The fragment-resolved spectrum is depicted in Figure 7. Four main photofragment ions are observed: $Fe(DXE)_2^+$, $Fe(OCH_3)_2(DXE)^+$, $Fe(CH_2O)(DXE)^+$, and $Fe(CO)(DXE)^+$. This spectrum was recorded with use of an attenuator (dividing the laser power by three), to avoid the presence of additional ions from further sequential fragmentation. Only two photofragments appear around 1970 cm^{-1}: $Fe(DXE)_2^+$ and $Fe(CO)(DXE)^+$, corresponding to the loss of CO and DXE ligands, respectively. The two other fragments are those obtained from photofragmentation of $Fe(DXE)_2^+$. This suggests the following fragmentation scheme:

$$Fe(CO)(DXE)_2^+ \rightarrow Fe(CO)(DXE)^+ + DXE$$

$$\rightarrow Fe(DXE)_2^+ + CO$$

In the 1970 cm^{-1} range, where $Fe(DXE)_2^+$ has no absorption band, no further fragmentation occurs. By contrast, the other bands of the $Fe(CO)(DXE)_2^+$ spectrum are also present in the spectrum of $Fe(DXE)_2^+$, so that $Fe(DXE)_2^+$ can absorb IR photons and fragment according to

$$Fe(DXE)_2^+ \rightarrow Fe(OCH_3)_2(DXE)^+ + CH_2{=}CH_2$$

$$Fe(OCH_3)_2(DXE)^+ \rightarrow Fe(CH_2O)(DXE)^+ + CH_3OH$$

In the 1050 cm^{-1} region $Fe(DXE)_2^+$ has a strong absorption band. Thus, the $Fe(DXE)_2^+$ ions produced by primary photofragmentation of $Fe(CO)(DXE)_2^+$ undergo light reabsorption and subsequent fragmentation as discussed above. This explains the particular shape of the $Fe(DXE)_2^+$ curve, showing an intensity depletion in the 1050−1080 cm^{-1} region where the absorption efficiency is highest for both $Fe(CO)(DXE)_2^+$ and $Fe(DXE)_2^+$ ions.

To check the proposed scheme, the number of macropulses has been varied for a fixed wavelength (1039 cm^{-1}). The branching ratio between $Fe(DXE)_2^+$ summed with its daughter ions, and $Fe(CO)(DXE)^+$, is plotted in Figure 8 against the number of macropulses. This branching ratio remains constant (0.61) with no visible trend, confirming that $Fe(DXE)_2^+$ and $Fe(CO)(DXE)^+$ are both primary fragments from the $Fe(CO)(DXE)_2^+$ ions. However, their branching ratio is observed to be dependent on the laser intensity: the proportion of $Fe(CO)(DXE)_2^+$ decreases at low laser intensity.

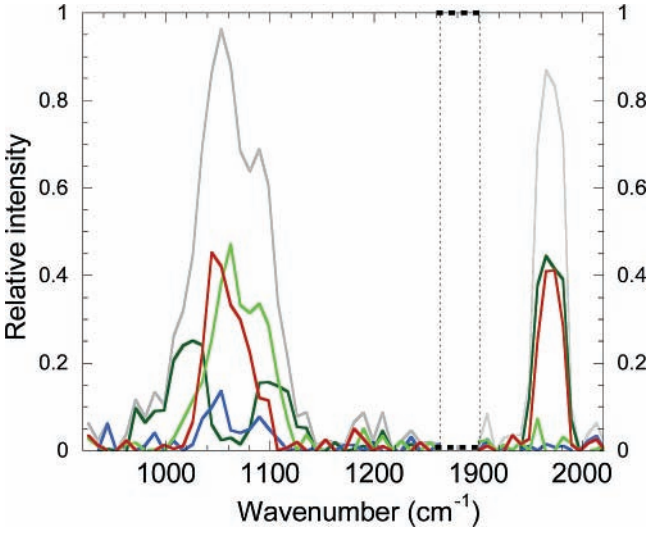

Figure 7. Evolution of the photofragments resulting from $Fe(CO)(DXE)_2^+$ as a function of energy (cm^{-1}). *m/z* 174, $Fe(CO)(DXE)^+$ (red); *m/z* 176, $Fe(CH_2O)(DXE)^+$ (green); *m/z* 208, $Fe(OCH_3)_2(DXE)^+$ (blue); *m/z* 236, $Fe(DXE)_2^+$ (dark green). The sum of the different photofragments is represented in gray.

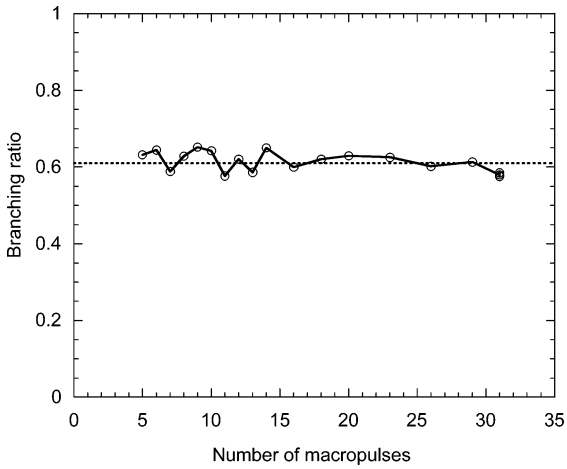

Figure 8. Evolution of the branching ratio $I_{Fe(DXE)^{2+}}/I_{Fe(DXE)^{2+}} + I_{Fe(CO)(DXE)^+}$ (each term referring to the intensity of the corresponding ion) between $Fe(DXE)_2^+$ (with its daughter ions) and $Fe(CO)(DXE)^+$ as a function of the number of macropulses. The dashed line indicates the average branching ratio value.

3. Thermochemistry. Ab initio calculations have been performed on iron complexes, to determine the thermochemistry of reactions experimentally observed. Results concerning $Fe(CO)_2^+$ [3] and $Fe(DXE)^+$ bound by one or two oxygen atom(s), as well as $Fe(DXE)_2^+$ bound by two, three, or four oxygen atoms[14] have been already published. Other structures have been calculated, among which the $Fe(CO)(DXE)^+$ (bound by one or two oxygen atom(s)) and $Fe(CH_2O)(DXE)^+$ (bound by two oxygen atoms) ions. Preliminary results are given below. Details of ab initio calculations will be published elsewhere. The main conclusions (concerning the reaction enthalpies at 0 K) are as follows:

•The substitution reaction of one CO by one DXE, when starting from the $Fe(CO)_2^+$ ion, is always an exothermic process, whatever the coordination mode of the dimethoxyethane.

•On the contrary, the substitution reaction of 2 CO by one DXE is always an endothermic reaction. However, this endothermicity is quite low (28 kJ mol^{-1}) when dimethoxyethane

SCHEME 3: First Step of the $Fe(DXE)^+ + DXE$ Reaction[a]

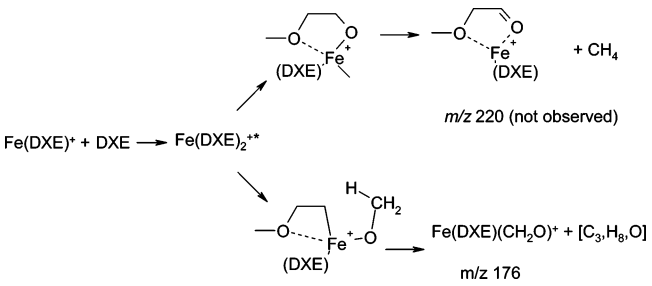

[a] The insertion of iron can be either in the $O-C_{Terminal}$ (upper part) or in the $O-C_{Central}$ (lower part) bond.

interacts with the metallic center with its two oxygen atoms. That is why this reaction is observed, as soon as $Fe(CO)_2^+$ ions have a small energy excess.

•The $Fe(CH_2O)(DXE)^+$ formation, when starting from $Fe(DXE)^+$ ions and DXE, is always an exothermic reaction, whatever the nature of neutrals in the reaction.

•The substitution reaction of methanal by DXE in the $Fe(CH_2O)(DXE)^+$ complex is exothermic when the four oxygen atoms interact with iron in the final $Fe(DXE)_2^+$ ion.

•When starting from $Fe(CO)(DXE)^+$, the formation of ion $Fe(CH_2O)(DXE)^+$ is either a thermoneutral reaction (7 kJ mol^{-1}) or an endothermic one (55 kJ mol^{-1}), depending on the nature of the neutral products: ethylmethyl ether, or ethene + methanol. This is consistent with the fact that the more argon there is in the reaction mixture, the less $Fe(CH_2O)(DXE)^+$ is detected.

The relevant reaction enthalpies are used for the construction of Scheme 5.

4. Mechanism of C—O Activation. 4.1. Regioselectivity. The first step of the reactions or fragmentations involving DXE activation is necessarily the insertion of the metal into a C−O bond of DXE. By contrast with DME, insertion may involve either of two nonequivalent sites, $O-C_{terminal}$ or $O-C_{central}$ bond. The nature of all the reaction or fragmentation products obtained indicates that the insertion which affords the products proceeds into the $O-C_{central}$ bond, as depicted in Scheme 3. Insertion in the $O-C_{terminal}$ bond would give a $RCH_2-O-Fe^+-CH_3$ intermediate leading to methane or methyl radical elimination, in analogy with the reactivity of DME complexes.[5] None of these channels has been observed in any of our experiments. The same regioselectivity (cleavage of the $O-C_{central}$ bond and not the $O-C_{terminal}$) has already been evidenced in the case of the $Fe^+ + CH_3(OCH_2CH_2)_3OCH_3$ system.[48] The observed regioselectivity may result from either of two possible mechanisms: (i) rate-determining iron insertion occurring preferentially into the $O-C_{central}$ bond, followed by fast dissociation of the inserted intermediate, (ii) reversible insertion of iron into one or both O−C bonds, followed by rate-determining dissociation which would be faster for the $O-Fe-C_{central}$ inserted intermediate than for the $O-Fe-C_{terminal}$ one.

4.2. Comparison of Ion−Molecule Reaction Products with IRMPD Products. While it could have been expected that IRMPD of $Fe(DXE)_2^+$ and ion−molecule reaction of $Fe(DXE)^+$ with DXE would lead to the same primary products, it is important to note that it is not the case: the ion−molecule reaction affords $Fe(CH_2O)(DXE)^+$ only (we have checked that this reaction does not give $Fe(OCH_3)_2(DXE)^+$ ions) and the $Fe(DXE)_2^+$ primary photofragmentation leads to $Fe(OCH_3)_2(DXE)^+$. Similarly, the $Fe(CO)(DXE)_2^+$ photofragmentation leads to the two products $Fe(DXE)_2^+$ and $Fe(CO)(DXE)^+$, while the nonassociative reaction of $Fe(CO)(DXE)^+$ with DXE gives three products as depicted in Scheme 1. As explained in the following, these differences are due to the energy dependence of the evolution of the excited intermediate ions involved, specifically $Fe(DXE)_2^+$*.

4.3. Mechanism of DXE Activation and Nature of the Neutral Products. The intermediate formed in the reaction of $Fe(DXE)^+$ with DXE results from insertion of the iron atom in the $O-C_{central}$ bond of DXE (Scheme 3). Two possible mechanisms for the evolution of this intermediate are shown in Scheme 4.

The two mechanisms differ in the nature of the neutral molecules formed: $CH_3OC_2H_5$ for the "A" mechanism and $CH_2=CH_2 + CH_3OH$ for the "B" mechanism.

The first mechanism is similar to the one proposed in the case of dimethyl ether complexes.[5] The initially formed ion−molecule complex may evolve through metal insertion in the $C_{central}-O$ bond of dimethoxyethane. The resulting species may then undergo an H atom transfer from the methoxy ligand leading to $Fe(DXE)(CH_2O)(CH_3CH_2OCH_3)^+$ and finally to the products $Fe^+(DXE)(CH_2O)$ and $CH_3OC_2H_5$. The formation of $CH_3OC_2H_5$ from $CH_2=CH_2 + CH_3OH$ is exothermic by 68 kJ·mol^{-1};[47] therefore, mechanism A corresponds to the most exothermic channel.

However, the second mechanism is much more likely when considering the whole set of data. It involves successive elimination of the neutrals $CH_2=CH_2$ and CH_3OH. The first step leads to excited $Fe(OCH_3)_2(DXE)^+$, which undergoes isomerization to $Fe(OCH_2)(CH_3OH)(DXE)^+$ followed by methanol loss. This is consistent with the $Fe(DXE)_2^+$ photofragmentation pathway, leading to $Fe(OCH_3)_2(DXE)^+$ as primary product and $Fe(DXE)(CH_2O)^+$ from its further fragmentation. In the Fe-

SCHEME 4: Two Possible Mechanisms for the $Fe(DXE)^+ + DXE \rightarrow Fe(CH_2O)(DXE)^+$ Reaction, Corresponding to Formation of Different Neutrals: $CH_3OC_2H_5$ for Mechanism A and $CH_2=CH_2 + CH_3OH$ for Mechanism B

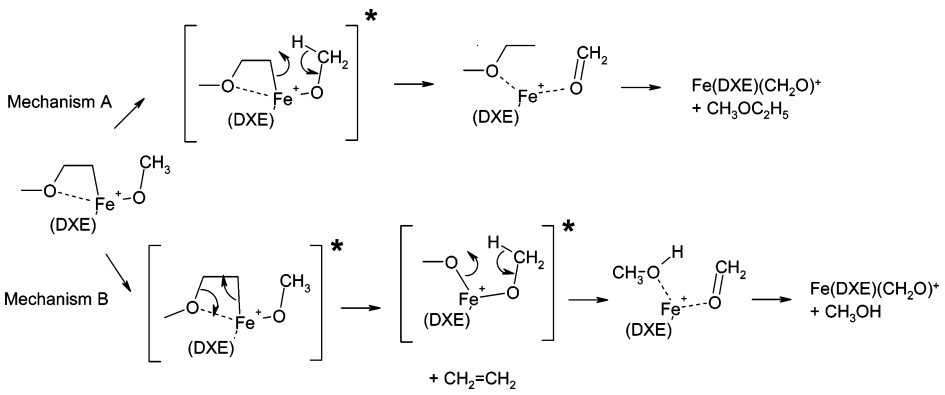

SCHEME 5: Energetics of the Different Ions Met in the $Fe(CO)_2^+$ + DXE System (Energies indicated in kJ mol^{-1})[a]

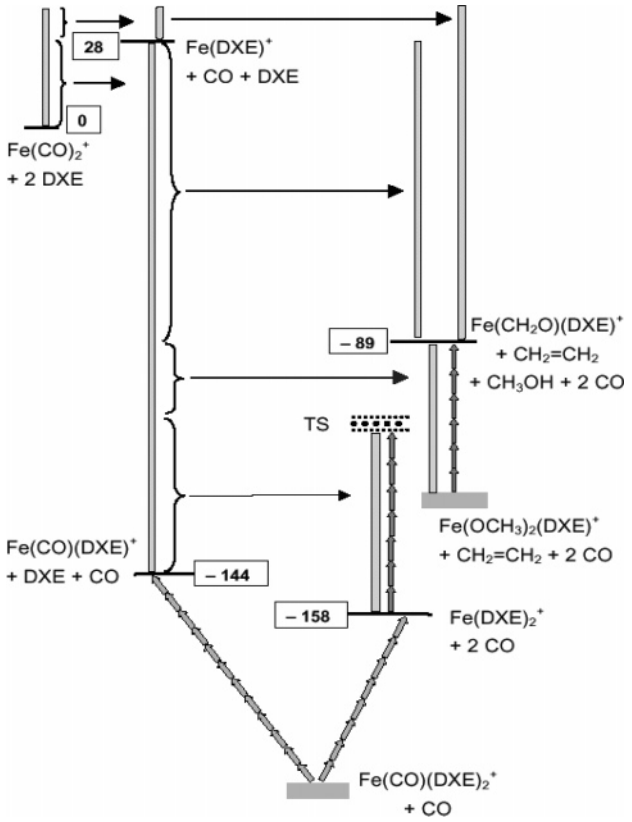

[a] The energies of the relevant systems, figured by thin horizontal bars, result from ab initio calculations, and refer to the ($Fe(CO)_2^+$ + 2 DXE) system taken as energy zero. The thermochemistry of $Fe(OCH_3)_2(DXE)^+$ and $Fe(CO)(DXE)_2^+$ has not been calculated yet. The approximate energy levels of the corresponding systems are figured by thick grey bars. The vertical rectangles indicate the energetic regions which can be reached by the corresponding reaction. The gray arrows show the fragmentation patterns observed in the IRMPD experiments.

$(DXE)^+$ + DXE ion−molecule system, the excited $Fe(OCH_3)_2(DXE)^+$ intermediate has enough energy for immediate methanol loss, leading directly to the $Fe(CH_2O)(DXE)^+$ ion.

The mechanism of the $Fe(DXE)^+$ + DXE reaction can therefore be described as the (B) mechanism, the neutrals produced being $CH_2{=}CH_2$ + CH_3OH.

4.4. Dependence of the Evolution of $Fe(DXE)_2^+$* with Its Internal Energy. The product distributions observed in the $Fe(CO)(DXE)^+$ + DXE reaction and in the sequential photofragmentation of $Fe(CO)(DXE)_2^+$ are compared as follows: $Fe(CO)(DXE)^+$ ions of high internal energy lead directly to $Fe(CH_2O)(DXE)^+$ (tertiary photofragmentation product); ions of intermediate energy give $Fe(OCH_3)_2(DXE)^+$ (secondary photofragmentation product), whereas ions of lower energy afford $Fe(DXE)_2^+$ (primary photofragmentation product).

The primary photofragmentation of $Fe(CO)(DXE)_2^+$ ions leads to $Fe(CO)(DXE)^+$ concurrently with $Fe(DXE)_2^+$. The DXE loss becomes the major channel when the laser power increases. This is consistent with thermochemistry since DXE is more strongly bound than CO to $Fe(DXE)^+$. This is also consistent with the fact that the rate of conversion of $Fe(CO)(DXE)^+$ to $Fe(DXE)_2^+$ is lower for "hot" $Fe(CO)(DXE)^+$ ions than for the "cold" ones (relaxation step in the kinetic modeling, and Figure 3): the proportion of DXE loss in $Fe(CO)(DXE)_2^+$ photofragmentation corresponds to the proportion of $Fe(CO)(DXE)_2^{+}$* intermediate going back to the $Fe(CO)(DXE)^+$ + DXE reactants in the ion−molecule reaction.

The energetics of the relevant systems are figured in Scheme 5. The reactive and photofragmentation pathways interconnecting these systems are summarized on the same scheme. For each reactive pathway an energy range is available for the product, since products with a lower energetic content than the reactants can be reached through collisional relaxation.

Yet no attempt has been made to get a more accurate characterization of the energy distribution of the reacting ions, for instance in terms of effective internal energy.[49,50] The effect of radiative or collisional relaxation on the effective internal energies (or the effective temperature) of the reactant and intermediate ions is an interesting point requiring further study.

Conclusion

The mechanism of C−O activation in the $Fe(DXE)^+$ + DXE system has been shown to involve ethene loss followed by methanol loss (Scheme 4B). This pathway is definitely different from the mechanism of C−O activation in the $Fe(DME)^+$/DME system, which proceeds by H transfer. A similar H transfer reaction in the $Fe(DXE)^+$ + DXE system (Scheme 4A), leading to the same $Fe(CH_2O)(DXE)^+$ product ion and ethylmethyl ether, would be more exothermic than the C−O activation pathway which is actually followed. Therefore, we come to the conclusion that the reaction is kinetically controlled and that the successive ethene and methanol losses involve lower activation barriers than those associated with H transfer leading to ethylmethyl ether loss. The nature of the IRMPD products of $Fe(DXE)_2^+$ has played a crucial role in this elucidation, since the gradual energy supply to the system allows to separate the two successive dissociation steps, while it is not possible in the direct $Fe(DXE)^+$ + DXE ion−molecule reaction.

The nature of the IRMPD fragmentation products also gives qualitative information about the dissociation energy barriers and the ligand effects associated with their heights. For instance, in $Fe(DXE)_2^+$ the barrier for ethene loss from the DXE ligand appears lower than the barrier for DXE loss, which is not observed. By contrast, in $Fe(CO)(DXE)_2^+$ ethene loss is not observed, showing that the corresponding barrier is higher than the barriers for the two possible ligand losses, i.e., DXE loss and CO loss which corresponds to the lowest energy.

The IRMPD results and the results of kinetic studies of ion−molecule reactions are consistent and complementary. While IRMPD probes the lowest energy dissociation channels, kinetic studies of ion−molecule reactions probe higher energy contents of the system.

The reactivity of the $Fe(CO)(DXE)^+$ + DXE system is particularly dependent on its energy content. Among the different reaction products, ion $Fe(OCH_3)_2(DXE)^+$ (*m*/*z* 208), obtained only within a restricted energy range, may call for further structural and reactivity studies due to the versatility of its binding mode. The energy dependence of the evolution of the $Fe(DXE)_2^{+}$* intermediate ion is thus remarkable in a relatively narrow energy range: a few tenths of an electronvolt. In this respect, the kinetic modeling method which consists of building a kinetic scheme using two or more species with different reactivities for the same intermediate ion, along with bayesian data analysis, appears as a very powerful tool in order to model and understand these energy-dependent reactions.

Acknowledgment. We thank Pierre Boissel, Joël Lemaire, and Philippe Maître for their contribution to the IRMPD studies. Ann McCluskey is thanked for English corrections.

References and Notes

(1) Cotton, F. A.; Wilkinson, G.; Murillo, C. A.; Bochmann, M. *Advanced Inorganic Chemistry*, 6th ed.; Wiley: New York, 1999; pp 27−29.

(2) Le Caër, S.; Heninger, M.; Mestdagh, H. *Chem. Phys. Lett.* **2002**, *352*, 393−400.

(3) Le Caër, S.; Heninger, M.; Maître, P.; Mestdagh, H. *Rapid Commun. Mass Spectrom.* **2003**, *17*, 351−357.

(4) Heninger, M.; Pernot, P.; Mestdagh, H.; Boissel, P.; Lemaire, J.; Marx, R.; Mauclaire, G. *Int. J. Mass Spectrom.* **2000**, *199*, 267−85.

(5) Le Caër, S.; Heninger, M.; Pernot, P.; Mestdagh, H. *Phys. Chem. Chem. Phys.* **2002**, *4*, 1855−1865.

(6) Le Caër, S.; Heninger, M.; Pernot, P.; Mestdagh, H. *C. R. Chimie* **2002**, *5*, 1−7.

(7) Heninger, M.; Pernot, P.; Mestdagh, H. *Chem. Phys. Lett.* **2001**, *333*, 358−364.

(8) Meot-Ner (Mautner), M.; Sieck, L. W.; Liebman, J. F.; Scheiner, S. *J. Phys. Chem.* **1996**, *100*, 6445−6450.

(9) Armentrout, P. B. *Int. J. Mass Spectrom.* **1999**, *193*, 227−240, and references therein.

(10) Guo, B. C.; Conklin, B. J.; Castleman, A. W., Jr. *J. Am. Chem. Soc.* **1989**, *111*, 6506−6510.

(11) Yang, X.; Castleman, A. W., Jr. *J. Chem. Phys.* **1990**, *93*, 2405−2412.

(12) Koizumi, H.; Armentrout, P. B. *J. Am. Soc. Mass Spectrom.* **2001**, *12*, 480−489.

(13) Shen, J.; Brodbelt, J. S. *Int. J. Mass Spectrom.* **1998**, *176*, 39−61.

(14) Le Caër, S.; Heninger, M.; Lemaire, J.; Boissel, P.; Maître, P.; Mestdagh, H. *Chem. Phys. Lett.* **2004**, *385*, 273−279.

(15) Ervin, K. M. *Chem. Rev.* **2001**, *101*, 391−444.

(16) Heninger, M.; Lemaire, J.; Mauclaire, G.; Fenistein, S.; Jullien, S.; Marx, R. *J. Chem. Phys.* **1994**, *101*, 1923−1929.

(17) Marx, R.; Mauclaire, G.; Fenistein, S.; Lemaire, J.; Heninger, M. *Int. J. Mass Spectrom. Ion Proc.* **1997**, *165*, 97−105.

(18) Lemaire, J.; Mouchère, F.; Heninger, M.; Fenistein, S.; Marx, R.; Mauclaire, G. *Int. J. Mass Spectrom. Ion Proc.* **1998**, *172*, 129−135.

(19) Jullien, S.; Lemaire, J.; Fenistein, S.; Heninger, M.; Mauclaire, G.; Marx, R. *Chem. Phys. Lett.* **1993**, *212*, 340.

(20) Beechem, J. M.; Ameloot, M.; Brand, L. *Chem. Phys. Lett.* **1985**, *120*, 466.

(21) Sivia, D. S. *Data Analysis: A Bayesian Tutorial*; Clarendon−Oxford University Press: Oxford, U.K., 1996.

(22) Su, T.; Chesnavich, W. J. *J. Chem. Phys.* **1982**, *76*, 5183.

(23) Miller, K. J. *J. Am. Chem. Soc.* **1990**, *112*, 8533−8542.

(24) Jaffe, R. L.; Smith, G. D.; Yoon, D. Y. *J. Phys. Chem.* **1993**, *97*, 12745−12751.

(25) Lemaire, J.; Boissel, P.; Heninger, M.; Mauclaire, G.; Bellec, G.; Mestdagh, H.; Simon, A.; Le Caër, S.; Ortega, J. M.; Glotin, F.; Maître, P. *Phys. Rev. Lett.* **2002**, *89*, 273002.

(26) Prazeres, R.; Glotin, F.; Insa, C.; Jaroszynski, D.; Ortega, J. M. *Eur. Phys. J. D* **1998**, *3*, 87−93.

(27) Mauclaire, G.; Lemaire, J.; Boissel, P.; Bellec, G.; Heninger, M. *Eur. J. Mass Spectrom.* **2004**, *10*, 155−162.

(28) Frisch, M. J.; Trucks, G. W.; Schlegel, H. B.; Scuseria, G. E.; Robb, M. A.; Cheeseman, J. R.; Zakrzewski, V. G.; Montgomery, J. A. J.; Stratmann, R. E.; Burant, J. C.; Dapprich, S.; Millam, J. M.; Daniels, A. D.; Kudin, K. N.; Strain, M. C.; Farkas, O.; Tomasi, J.; Barone, V.; Cossi, M.; Cammi, R.; Mennucci, B.; Pomelli, C.; Adamo, C.; Clifford, S.; Ochterski, J.; Petersson, G. A.; Ayala, P. Y.; Cui, Q.; Morokuma, K.; Malick, D. K.; Rabuck, A. D.; Raghavachari, K.; Foresman, J. B.; Cioslowski, J.; Ortiz, J. V.; Stefanov, B. B.; Liu, G.; Liashenko, A.; Piskorz, P.; Komaromi, I.; Gomperts, R.; Martin, R. L.; Fox, D. J.; Keith, T.; Al-Laham, M. A.; Peng, C. Y.; Nanayakkara, A.; Gonzalez, C.; Challacombe, M.; Gill, P. M. W.; Johnson, B.; Chen, W.; Wong, M. W.; Andres, J. L.; Gonzalez, C.; Head-Gordon, M.; Replogle, E. S.; Pople, J. A. Gaussian 98; GAUSSIAN98 (Revision A.6); Gaussian, Inc.: Pittsburgh, PA, 1998.

(29) Bauschlicher, C. W. *Theor. Chim. Acta* **1995**, *92*, 183−198.

(30) Hay, P. J. *J. Chem. Phys.* **1977**, *66*, 4377−4384.

(31) Milliet, A.; Sozzi, G.; Audier, H. E. *Org. Mass Spectrom.* **1992**, *27*, 787−794.

(32) Johnstone, R. A. W.; Rose, M. E. *Tetrahedron* **1979**, 2169−2173.

(33) Drahos, L.; Vékey, K. *J. Mass Spectrom.* **2001**, *36*, 237−263.

(34) Drahos, L.; Sztaray, J.; Vékey, K. *Int. J. Mass Spectrom.* **2003**, *225*, 233−248.

(35) Prüsse, T.; Fiedler, A.; Schwarz, H. *J. Am. Chem. Soc.* **1991**, *113*, 8335−8339.

(36) Schalley, C. A.; Wesendrup, R.; Schröder, D.; Weiske, T.; Schwarz, H. *J. Am. Chem. Soc.* **1995**, *117*, 7711−7718.

(37) Fiedler, A.; Schröder, D.; Schwarz, H.; Tjelta, B. L.; Armentrout, P. B. *J. Am. Chem. Soc.* **1996**, *118*, 5047−5055.

(38) Kapota, C.; Lemaire, J.; Maître, P.; Ohanessian, G. *J. Am. Chem. Soc.* **2004**, *126*, 1836−1842.

(39) Jones, W.; Boissel, P.; Chiavarino, B.; Crestoni, M. E.; Fornarini, S.; Lemaire, J.; Maître, P. *Angew. Chem., Int. Ed. Engl.* **2003**, *42*, 2057−2059.

(40) Lemaire, J.; Boissel, P.; Heninger, M.; Mestdagh, H.; Mauclaire, G.; Le Caër, S.; Ortega, J.-M.; Maître, P. *Spectr. Anal.* **2003**, *32*, 28−31.

(41) Maître, P.; Le Caër, S.; Simon, A.; Lemaire, J.; Mestdagh, H.; Heninger, M.; Mauclaire, G.; Boissel, P.; Ortega, J.-M.; Prazeres, R.; Glotin, F. *Nucl. Instrum. Methods Phys. Res. A* **2003**, *507*, 541−546.

(42) van Heijnsbergen, D.; von Helden, G.; Meijer, G.; Maître, P.; Duncan, M. A. *J. Am. Chem. Soc.* **2002**, *124*, 1562−1563.

(43) Asmis, K. R.; Pivonka, N. L.; Santambrogio, G.; Brümmer, M.; Kaposta, C.; Neumark, D. M.; Wöste, L. *Science* **2003**, *299*, 1375−1377.

(44) Oomens, J.; Moore, D. T.; von Helden, G.; Meijer, G.; Dunbar, R. C. *J. Am. Chem. Soc.* **2004**, *126*, 724−725.

(45) Jaeger, T. D.; Fielicke, A.; von Helden, G.; Meijer, G.; Duncan, M. A. *Chem. Phys. Lett.* **2004**, *392*, 409−414.

(46) Schalley, C. A.; Wesendrup, R.; Schröder, D.; Schroeter, K.; Schwarz, H. *J. Am. Chem. Soc.* **1995**, *117*, 12235−12242.

(47) Afeefy, H. Y.; Liebman, J. F.; Stein, S. E. Neutral Thermochemical Data. In *NIST Chemistry WebBook, NIST Standard Reference Database Number 69*; Linstrom, P. J., Mallard, W. G., Eds.; National Institute of Standards and Technology: Gaithersburg MD, 20899 (http://webbook.nist.gov), March 2003.

(48) Huang, S. K.; Allison, J. *Organometallics* **1983**, *2*, 883−890.

(49) Vékey, K. *J. Mass Spectrom.* **1996**, *31*, 445−463.

(50) Norrman, K.; McMahon, T. B. *Int. J. Mass Spectrom.* **1998**, 87−97.